CHINESE OPTICS LETTERS

Vol. 22, No. 4 | April 2024

Design of a high frequency accuracy heterodyne laser source working in a wide temperature range

Hongxing Yang (杨宏兴)[1,2], Yan Wang (王 彦)[1,2], Ziqi Yin (殷子淇)[1,2], Pengcheng Hu (胡鹏程)[1,2*], Ruitao Yang (杨睿韬)[1,2], and Jing Li (李 婧)[1,2]

[1] Center of Ultra-precision Optoelectronic Instrument, Harbin Institute of Technology, Harbin 150080, China

[2] Key Laboratory of Ultra-precision Intelligent Instrumentation (Harbin Institute of Technology), Ministry of Industry and Information Technology, Harbin 150080, China

*Corresponding author: hupc@hit.edu.cn

Received October 10, 2023 | Accepted January 6, 2024 | Posted Online April 25, 2024

To ensure the frequency accuracy of a heterodyne laser source in the ambient temperature range of −20°C to 40°C, a dual-longitudinal-mode thermally stabilized He–Ne laser based on non-equilibrium power locking was designed. The ambient adaptive preheating temperature setting scheme ensured the laser could operate normally in the range of −20°C to 40°C. The non-equilibrium power-locked frequency stabilization scheme compensated for the frequency drift caused by different stabilization temperatures. The experimental results indicated that the frequency accuracy of the laser designed in this study could reach 5.2×10^{-9} in the range of −20°C to 40°C.

Keywords: He–Ne laser; frequency accuracy; ambient adaptability; non-equilibrium power locking.
DOI: 10.3788/COL202422.041407

1. Introduction

Due to noncontact, high measurement accuracy, high dynamic measurement range, and the fact that the measurement results can be directly traced back to the length reference, laser interference displacement measurement techniques and instruments have been widely used in the fields of ultraprecision equipment processing and manufacturing. Laser interferometers also play an important role in ocean exploration, geodesy, geophysics, and national security. Laser interferometers in these areas are often faced with harsh external environments, and they are required to have a certain degree of measurement accuracy, which poses a serious challenge to the laser interferometers[1–3].

Taking the laser interferometric absolute gravity meter as an example, to obtain accurate gravity values at different locations in the world, they must perform accurate measurements in field environments to provide data support for scientific research. The current method of ensuring the accuracy of laser interferometers is to keep them warm until they are at a normal temperature, which undoubtedly greatly increases the cost of manpower and time costs[4,5].

As the measurement basis of the laser interferometer, the frequency accuracy, stability, and environmental adaptability of the laser source directly determine its working accuracy under severe environments. Owing to their direct traceability, narrow linewidth, and easily being frequency-stabilized, He–Ne lasers have been widely studied and applied in laser interferometers.

At present, He–Ne laser frequency stabilization methods mainly include iodine molecule saturation absorption frequency stabilization and dual longitudinal mode thermal frequency stabilization. Although the iodine saturation absorption frequency stabilization method has high frequency stabilization accuracy, its long preheating time and temperature characteristics of the iodine molecule make it difficult to apply to rapid field measurements. Dual longitudinal mode thermal frequency stabilization has a simple structure and no modulation output, but its working environment is also mainly concentrated in the laboratory or industrial site; otherwise the laser will produce frequency drift or even cannot work properly. Although researchers have proposed techniques such as water cooling and air cooling to ensure a stable thermal environment and reduce the thermal pollution of the laser tube, they have not been able to effectively extend the laser's operating temperature[6–8].

This study took the dual longitudinal mode thermally stabilized He–Ne laser as the research object, and investigated the drift characteristics of the laser's frequency with the ambient temperature in the temperature range of −20°C to 40°C. Then, ambient adaptive preheating temperature setting scheme and nonequilibrium power-locked frequency stabilization scheme were proposed to ensure the He–Ne laser frequency stability and accuracy.

2. Principle

2.1 Preheating setting scheme

The normal working process of the laser can be divided into two parts: preheating and frequency stabilization. The purpose of preheating is to establish approximate thermal equilibrium between the laser and the environment, which is a prerequisite for entering the frequency stabilization control process.

When a laser is free-running in the absence of electric heating film conditions, it reaches thermal equilibrium with the ambient temperature after a period of time and maintains a certain temperature difference that is caused by the self-heating power. As shown in Fig. 1(a), the boundary temperature of the laser tube and the thermal structure is approximately equal ($T_1 = T_2$) when the heat balance is established.

Assume that the thermal energy with power P_t is emitted to the air environment, according to the energy balance equation,

$$P_t = 2\pi r_2 lh(T_2 - T_A). \tag{1}$$

T_A is the ambient temperature, l is the length of the laser tube, and h is the convective heat transfer coefficient. Then the laser tube temperature during thermal balance is

$$T_2 = \frac{P_t}{2\pi r_2 lh} + T_A. \tag{2}$$

In this design, the self-heating power is $P_t = 6\,\mathrm{W}$. When $h = 25\,\mathrm{W/(m^2 \cdot K)}$, $r_2 = 0.013\,\mathrm{m}$, and $l = 150\,\mathrm{mm}$, the increased temperature caused by the self-heating effect is 19.56°C.

This study used a high- and low-temperature test chamber (temperature adjustment range, −25°C to 150°C; temperature adjustment accuracy, 0.5°C) to simulate the ambient temperature, and the temperature measured by the external laser temperature sensor TS_3 (PT1000; temperature measurement accuracy, 0.005°C) was set as the actual ambient temperature value (T_A). The laser was subjected to free-running experiments at seven different ambient temperature points for at least 6 h each. The data were recorded, as shown in Fig. 1(b). The laser maintained a temperature difference of approximately 20°C with the environment after free-running to reach thermal equilibrium in the range of −20°C to −40°C, which was consistent with the above analysis.

Because the electrothermal film can only increase thermal energy and adjust the cavity length monotonically, to establish a controllable thermal equilibrium state, the laser preheating temperature should be higher than its free-running temperature. Considering the power of the heated film and the limit of the laser tube operating temperature (approximately 70°C), the preheating temperature (T_{set}) was set as 25°C higher than the ambient temperature,

$$T_{set} = T_A + 25. \tag{3}$$

This can effectively solve the problem encountered under the traditional fixed preheating temperature solution, in which it is difficult to establish an effective thermal equilibrium state when the ambient temperature is too low or too high, resulting in the laser not operating properly and accurately.

2.2. Preheating temperature control scheme

To ensure the accuracy of the laser preheating temperature, researchers from the Harbin Institute of Technology have proposed a preheating temperature control scheme based on longitudinal mode-hopping feedback. In this scheme, every time the laser cavity length changes by $\lambda/2$, where λ is the laser wavelength, the longitudinal mode number changes by 1. Owing to the low thermal expansion coefficient of the laser tube, the temperature change (ΔT_{mod}) required for the laser tube to change one mode remains almost constant under different ambient temperatures[9]. ΔT_{mod} can be calculated by Eq. (4),

$$\Delta T_{mod} = \frac{\lambda/2}{\alpha L}, \tag{4}$$

where α is laser tube thermal expansion coefficient. For a laser tube with a wavelength of 633 nm, a length of 150 mm, and a thermal expansion coefficient of approximately $3.0 \times 10^{-6}\ °C^{-1}$, ΔT_{mod} is approximately 0.7°C.

After the laser is powered up, the number of longitudinal modes (N) that must be changed for the laser cavity to reach the preset temperature can be obtained from the laser cavity temperature (T_{tube}) and the preheating set temperature (T_{set}).

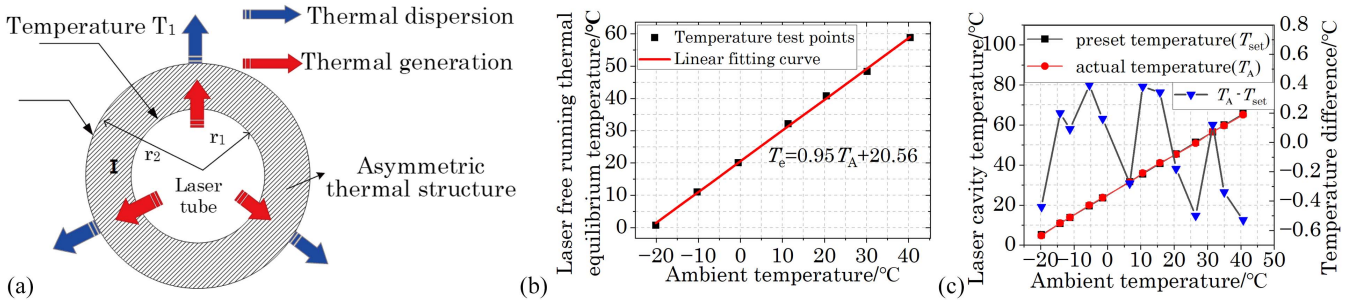

Fig. 1. (a) Thermal equilibrium state; (b) thermal equilibrium temperature of the laser free-running experiment; (c) comparison of the preset temperature and actual temperature of the laser cavity.

Because N takes only a positive integer, there is an error of ±1 when N is calculated using Eq. (5); hence, there is an error of $\pm\Delta T_{\mathrm{mod}}$ between the actual preheating temperature of the laser tube and the set temperature,

$$N = \frac{T_{\mathrm{set}} - T_{\mathrm{tube}}}{\Delta T_{\mathrm{mod}}}. \tag{5}$$

In this study, 13 ambient temperature points were selected in the range of −20°C to 40°C for preheating control using the longitudinal mode-hopping feedback preheating temperature control scheme. The laser cavity preset temperature and actual preheating temperature, as well as the difference between the two obtained are shown in Fig. 1(c). This scheme effectively controlled the laser cavity temperature within the range of ±0.6°C from the preset temperature, which guaranteed laser frequency repeatability at the same ambient temperature point[10].

2.3. Nonequilibrium power-locked frequency stabilization scheme

Although the preheating temperature control scheme guarantees frequency repeatability at the same ambient temperature point, the problem of laser frequency drift still exists. This is because the output frequency accuracy depends, to a certain extent, on the laser preheating temperature. The laser output frequency will drift with the difference in the preheating temperature.

The frequency difference of the two modes depends primarily on the mode spacing and is affected by the mode pulling and pushing effects. The laser output beam frequency is

$$f = m\frac{c}{2nL}, \tag{6}$$

where c is the light velocity in vacuum, L is the cavity length, n is the refractive index inside the laser tube, and m is the laser mode number. From Eq. (6), the frequency accuracy is

$$\left|\frac{\Delta f}{f}\right| = \frac{\Delta L}{L} + \frac{\Delta n}{n}, \tag{7}$$

where $\Delta L/L$ is the fractional change in the cavity length and $\Delta n/n$ is the fractional change in the refractive index.

However, the center frequency of the Doppler width varies with the pressure inside the tube with a rate of 18 MHz/Torr[11]. Hence, the Eq. (7) is changed in

$$\left|\frac{\Delta f}{f}\right| = \frac{\Delta L}{L} + \frac{\Delta n}{n} + \frac{\Delta f_0}{f_0}, \tag{8}$$

where $\Delta f_0/f_0$ is the fractional change of the center frequency against the pressure of the gas inside the laser tube[12].

Meanwhile, the pressure in the laser tube changes linearly with the temperature, which explains why the laser frequency drifts in the range of −20°C to 40°C. Related research pointed out the drift rate was approximately 0.2–0.6 MHz/°C[13].

To further verify the output frequency drift with temperature, experiments on beat frequency with an iodine-stabilized laser (ISL) were performed at 13 temperature points, shown in Fig. 1(c). To isolate vibration, the beat frequency device including ISL and the constant temperature box are not in the same room. The data were collected using the frequency counter 53230A (Agilent Technologies, Santa Clara, USA) with a sampling time of 0.1 s. The beat frequency at each temperature point was maintained not less than 3 h; the experimental results are shown in Fig. 2(a). The laser frequency drift peak-to-peak value was approximately 16.2 MHz within −20°C to 40°C, and the laser frequency accuracy was only 3.4×10^{-8}.

According to Eq. (6), the frequency difference between neighboring longitudinal modes is

$$\Delta f = \frac{c}{2nL}. \tag{9}$$

This study used a 150 mm laser tube. Δf is approximately 1000 MHz, calculated from Eq. (9). The He–Ne laser gain curve bandwidth is approximately 1500 MHz, so there are only two longitudinal modes in the laser tube that can form laser light, and the two longitudinal modes are located on both sides of the gain curve center. The equilibrium power frequency stabilization strategy achieves frequency stabilization by controlling the two longitudinal modes' optical power to be symmetrical about the gain curve. The nonequilibrium power frequency

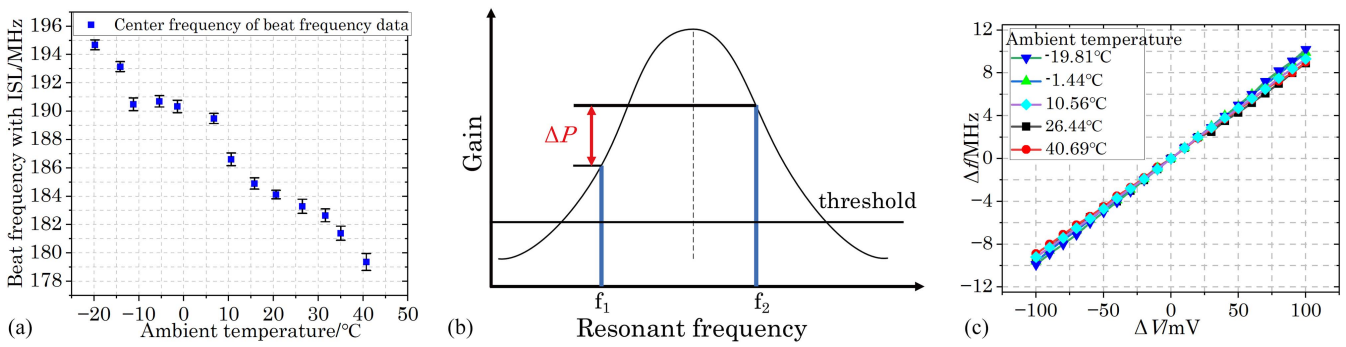

Fig. 2. (a) Laser beat frequency at different temperatures; (b) nonequilibrium power-locking principle; (c) variation in laser frequency with error signal.

stabilization control scheme no longer takes the zero point of the power difference as the frequency stabilization reference but controls the power of the two longitudinal modes within a small range of a certain deviation ΔP, as shown in Fig. 2(b). Owing to the correspondence between laser frequency and power, the laser frequency can be corrected by adjusting the value of ΔP at different temperatures to ensure it is close to the same frequency and improve the frequency accuracy.

To correct the reference point of laser frequency stabilization more accurately, the relationship between laser frequency and temperature and the relationship between laser frequency and optical power must be determined.

In Fig. 2(a), the laser center frequency drift with temperature followed a relatively clear linear trend. However, to ensure the accuracy of the laser frequency versus temperature model, this study adapted a segmented linear fit to calculate this model, with the temperature interval set as $[-20.01, -11.25)$, $[-11.25, 6.69)$, $[6.69, 15.75)$, $[15.75, 31.56]$, and $[31.56, 40.69]$.

Because the commercial He–Ne laser tube parameters cannot be known, a specific expression for the laser gain curve cannot be directly obtained. Therefore, it is necessary to establish a model for the variation in laser frequency with power through experiments:

$$f = \begin{cases} f_F - 185.81 + 0.462T_A & -20.01 \le T_A < -11.25 \\ f_F - 190.09 + 0.06T_A & -11.25 \le T_A < 6.69 \\ f_F - 192.48 + 0.497T_A & 6.69 \le T_A < 15.75 \\ f_F - 187.1 + 0.142T_A & 15.75 \le T_A < 31.56 \\ f_F - 194.01 + 0.360T_A & 31.56 \le T_A \le 40.69 \end{cases}. \tag{10}$$

The laser power P was converted into a voltage signal after acquisition by the detector, I/V conversion, filtering, and amplification circuits. Therefore, the optical power deviation ΔP can be expressed as an error signal as follows:

$$\Delta V = k \cdot \Delta P, \tag{11}$$

where k is the conversion factor. The correction of the output frequency can be realized by modifying the error signal ΔV value in the closed-loop feedback control. In this study, the variation in the laser center frequency under equilibrium power frequency stabilization control was observed for every 10 mV change in ΔV at five different ambient temperature points, as shown in Fig. 2(c). The laser center frequency changed linearly with the error signal at each temperature point, but the linear curve sensitivity was slightly different at different temperatures. The sensitivity in order of temperature from low to high was 0.10 MHz/mV, 0.097 MHz/mV, 0.093 MHz/mV, 0.090 MHz/mV, and 0.089 MHz/mV, which served as the sensitivity of the amount of frequency variation to the amount of voltage variation for the five temperature bands.

Thus far, this study has established a variation model of laser frequency with ambient temperature and a variation model of laser frequency with error signal.

3. Experiment

3.1. Experiment setup

The structural design scheme is illustrated in Fig. 3(a). The microcontroller unit (MCU) detects the ambient temperature via the external temperature sensor TS_3 and sets the preheating temperature according to the ambient temperature. During the warm-up stage, the MCU collects the optical power signal which is spectrally divided by a Wollaston prism and converted into a voltage signal by a photodetector (PD), current to voltage conversion (I/V), and analog-to-digital conversion (A/D) to calculate the change of the longitudinal mode stage number. Meanwhile, the MCU drives digital-to-analog conversion (D/A) and the power amplifier (P-AMP) to achieve laser tube heating. After entering the frequency stabilization phase, the current output frequency value is calculated by the MCU according to the ambient temperature, and the error signal ΔV is calculated according to the difference between the current frequency and the preset frequency. Then the MCU uses ΔV as a feedback signal to control the power difference between the two longitudinal modes near ΔP for laser frequency correction.

Based on the structural scheme, the laser frequency stabilization system was designed and is shown in Fig. 3(b).

In addition, to minimize the error on frequency stabilization control caused by the optical components temperature drift, the optical components used in this study had good temperature stability, for example, true zero-order half-wave plates were used. Moreover, two-element Si PIN photodiodes were used as PDs, which had good performance consistency; its sensitivity at 633 nm did not change with temperature. And the selected circuit components tolerable operating temperature range was concentrated at −40°C to 125°C to meet the requirements of use.

3.2. Experiment results

Using the above scheme, six temperature points were selected in the range of −20°C to 40°C to conduct beat frequency experiments on the designed laser with ISL. The ISL vacuum wavelength relative expansion uncertainty is 5.0×10^{-11} ($k = 3$) (calibration certificate number CDcd2022-00002). According to the 633 nm frequency-stabilized laser calibration regulations (specification number: JJG 353-2006), each beat frequency time was 3 h; the results are shown in Figs. 4(a)–4(f). At the same time, we calculated the laser frequency Allan variance at different temperatures, as shown in Table 1.

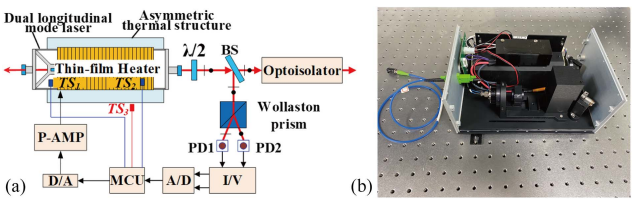

Fig. 3. (a) Structural solution of laser; (b) frequency stabilization system.

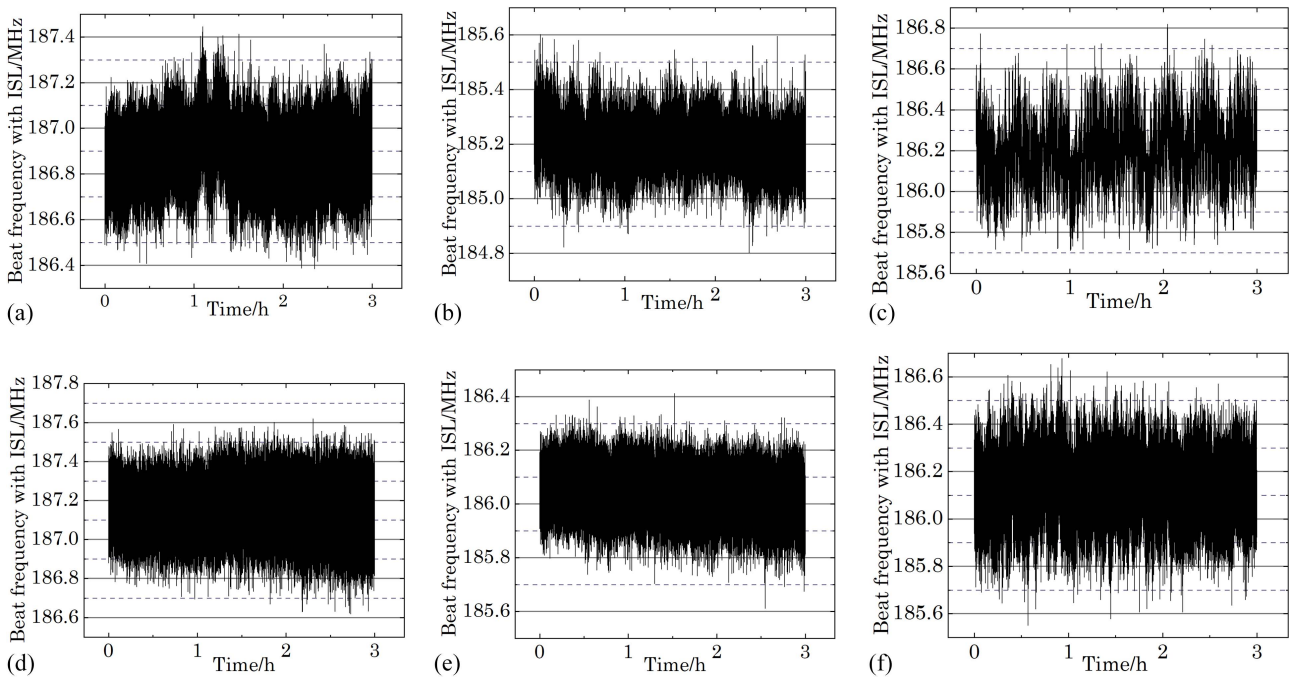

Fig. 4. Beat frequency with ISL at different ambient temperatures. (a) −20.13°C, (b) −9.22°C, (c) 8.64°C, (d) 16.13°C, (e) 28.32°C, (f) 40.13°C.

Table 1. Allan Variance of Laser Frequency Stabilization at Different Temperatures.

	Ambient Temperature/°C					
Sampling Time/s	−20.13	−9.22	8.64	16.13	28.32	40.13
0.1	2.44×10^{-10}	7.51×10^{-11}	6.39×10^{-11}	3.29×10^{-10}	4.40×10^{-10}	1.17×10^{-10}
1	6.40×10^{-11}	1.15×10^{-10}	3.41×10^{-11}	1.14×10^{-10}	1.65×10^{-10}	1.32×10^{-10}
10	3.97×10^{-11}	3.98×10^{-11}	5.07×10^{-11}	3.41×10^{-11}	5.14×10^{-11}	4.00×10^{-11}
100	5.28×10^{-11}	2.53×10^{-11}	5.22×10^{-11}	1.58×10^{-11}	4.37×10^{-11}	6.74×10^{-11}
1000	6.12×10^{-11}	2.85×10^{-11}	3.17×10^{-11}	2.52×10^{-11}	5.44×10^{-11}	2.33×10^{-11}

Combining Figs. 4(a)–4(f) and Table 1, it can be seen that the laser beat frequency varied by no more than ±0.6 MHz@3 h at any temperature point over the entire temperature range, while the frequency stability based on the Allan variance had no large fluctuation.

The frequency plots at the six temperatures are shown in Fig. 5(a) in the form of error bars. The maximum laser frequency deviation δf was 2.5 MHz. Compared with previously measured frequency data in Fig. 2(a), the frequency accuracy was significantly improved, with a value of

$$R = \delta f / \left(\sum_{i=1}^{6} f_i / 6 \right) \approx 5.2 \times 10^{-9}. \tag{12}$$

Based on this method, two other lasers were designed. In Fig. 5(b), the frequency accuracy of these two lasers in the range of −20°C to 40°C can also reach 5.2×10^{-9}.

4. Discussion

In the preheating stage, the preheating temperature setting is very important. However, due to the limitation power of electrothermal film, the laser cannot be stabilized at the same temperature within the range of −20°C to 40°C, which is also the reason for the poor frequency accuracy of ordinary lasers. In this study, to ensure that the laser tube had the same thermal balance state at each preheating temperature, we set a fixed temperature difference between the preheating temperature and the ambient temperature so that the PID parameters of the frequency stabilization control program did not need to be modified with the change of the ambient temperature. In addition, there was a nearly linear relationship between the frequency stabilization temperature and the laser frequency in Fig. 2(a). Therefore, we established the relationship model between laser frequency and temperature by curve fitting, but the model accuracy

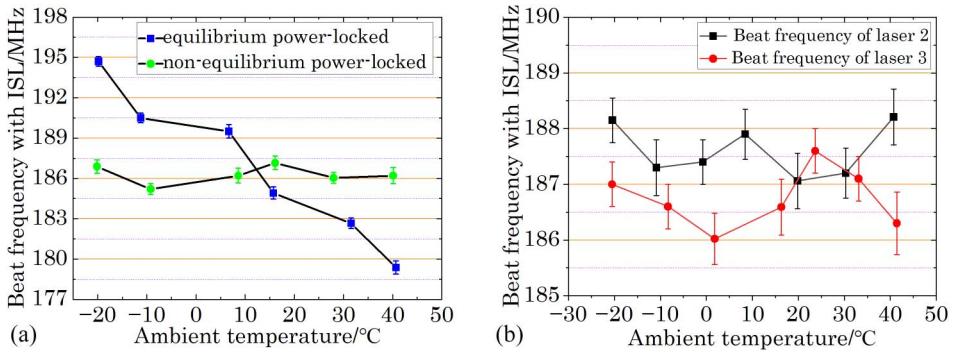

Fig. 5. (a) Comparison of nonequilibrium power and equilibrium power frequency stabilization schemes; (b) beat frequencies of the other two lasers at different temperatures.

depends on the number of test points and the model building method. The more test points and the more appropriate the modeling method, the more accurate models, but it also brings more work.

For the dual-longitudinal-mode He–Ne lasers, the variation model of laser frequency and optical power has obvious temperature dependence. This is because the Doppler linewidth of the laser gain curve shifts with the temperature of the resonator, resulting in a change in the slope of the gain curve at the equilibrium power point. Most He–Ne laser tubes have this characteristic. Therefore, the proposed nonequilibrium power-locked frequency stabilization scheme has a wide range of applicability in dual-longitudinal-mode thermally stabilized He–Ne lasers. Furthermore, to further improve the frequency compensation accuracy, a more accurate relationship model of laser frequency, light power, and ambient temperature should be established.

5. Conclusion

In conclusion, this study provided a new approach for improving the frequency accuracy of dual-longitudinal-mode thermally stabilized He–Ne lasers. The ambient adaptive preheating temperature setting scheme set the preheating working temperature based on the ambient temperature, which solved the limitations of the traditional fixed preheating temperature scheme and effectively expanded the laser working temperature range. Based on the nonequilibrium power-locked frequency stabilization control scheme, the relationship model between laser frequency and temperature, and the relationship model between laser frequency and optical power, were established through a combination of experiments and theory, which finally improved the frequency accuracy of the laser by 6 times compared with the equilibrium power frequency stabilization scheme.

Acknowledgements

This work was supported by the National Natural Science Foundation of China (Nos. 52175500, 52175501, and 52061135114).

References

1. Y. Bai, P. C. Hu, Y. F. Lu, *et al.*, "A six-axis heterodyne interferometer system for the joule balance," IEEE Trans. Instrum. Meas. **66**, 1579 (2017).
2. H. Yang, Z. Yin, X. Wang, *et al.*, "Design for a highly anti-interference He-Ne laser with novel multi-layer weakly coupled heat dissipation structure," Opt. Laser Technol. **156**, 108588 (2022).
3. M. Pisani, A. Yacoot, and P. Balling, "Comparison of the performance of the next generation of optical interferometers," Metro-logia **49**, 455 (2012).
4. https://microglacoste.com/wp-content/uploads/2021/02/A-10-Manual-web.pdf.
5. https://www.microglacoste.com/pdf/ml1-manual.pdf.
6. J. Qian, Z. Liu, C. Shi, *et al.*, "Frequency stabilization of internal-mirror He–Ne lasers by air cooling," Appl. Opt. **51**, 6084 (2012).
7. H. Yang, R. Yang, P. Hu, *et al.*, "Ultrastable offset-locked frequency-stabilized heterodyne laser source with water cooling," Appl. Opt. **56**, 9179 (2017).
8. Z.-B. Wang, J. Zhang, L.-J. Liu, *et al.*, "Water cooling technology on high power LED with the twisted tube," Acta Photon. Sin. **42**, 1350 (2013).
9. X. Diao, J. Tan, P. Hu, *et al.*, "Frequency stabilization of an internal mirror He–Ne laser with a high frequency reproducibility," Appl. Opt. **52**, 456 (2013).
10. T. M. Niebauer, J. E. Faller, H. M. Godwin, *et al.*, "Frequency stability measurements on polarization-stabilized He–Ne lasers," Appl. Opt. **27**, 1285 (1988).
11. G. S. Sasagawa and M. A. Zumberge, "Five-year frequency stability of a Zeeman stabilized laser," Appl. Opt. **28**, 824 (1989).
12. G. Budzyn, T. Podzorny, and J. Tkaczyk, "Method of improving the frequency repeatability of the intensity stabilized HeNe laser," Laser Phys. **25**, 065002 (2015).
13. M. A. Zumberge, "Frequency stability of a Zeeman-stabilized laser," Appl. Opt. **24**, 1902 (1985).